Predator-prey dynamics in a uniform medium lead to directed percolation and wave-train propagation

Alexandra Agranovich and Yoram Louzoun*
Department of Mathematics and Gonda Brain Research Center, Bar-Ilan University, Ramat Gan 52900, Israel
(Received 15 December 2011; published 21 March 2012)

The dynamics of birth-death processes with extinction points that are unstable in the deterministic average description has been extensively studied, mainly in the context of the stochastic transition from the mean-field attracting fixed point to the absorbing state. Here we study the opposite case of a small perturbation from the zero-population absorbing state. We show that such perturbations can grow beyond the mean-field attracting fixed point and then can collapse back into the absorbing state. Such dynamics can represent, for example, the fast growth of a pathogen and then its destruction by the immune system. We show that when the prey perturbation extinction probability is high, the loss of synchronization between the prey densities in different regions in space leads to two possible dynamic regimes: (a) a directed percolation regime based on the balance between regions escaping the absorbing state and regions absorbed into it, and (b) wave trains representing the transition of the entire space to the mean-field stable positive fixed point.

DOI: 10.1103/PhysRevE.85.031911 PACS number(s): 87.10.−e

I. INTRODUCTION

In the early 1920's, Lotka and Voltera showed that a system containing negative feedback of a predator on a prey can lead to sustained oscillations [1–4]. This observation, as expressed through the now classical Lotka-Voltera (LV) predator-prey (PP) equations, has been extensively studied. The original LV model has been enlarged to include more complex interaction terms [5–13], spatial heterogeneity [9,11,14–17], (for a review, see Ref. [18]), and stochastic interactions [19–27]. In discrete stochastic models, the LV model also has absorbing states of zero predator and prey or zero predator and either finite or infinite prey populations. In a deterministic continuous system, either the fixed point equivalent of the stochastic absorbing state is unstable and then each trajectory that leaves it reaches the stable fixed point, or it is stable and small perturbations exponentially decrease. Here we show, by using an application of the LV model to the interaction between the immune system and pathogens (ISP), the possibility of other regimes in discrete stochastic realizations of LV systems.

The model we study is an abstraction of the lymphocyte-pathogen dynamics. Lymphocytes have a pathogen-independent basal production rate in the bone marrow or in the thymus [28], and basal division and death rates. Upon infection, a few clones of pathogen-specific lymphocytes grow and destroy the pathogen, until the pathogen is eventually eradicated, within days or weeks [29]. Once the pathogen disappears, the lymphocyte clone size decays. The decay can either be to a basal level, or to a slightly higher level, if memory cells are formed [30–34]. These interactions can be summarized by the following reactions: (a) proliferation of the pathogen x with a rate of α; (b) duplication of host lymphocytes in response to an encounter with a pathogen with a rate of ν; (c) pathogen destruction by the host lymphocytes with a rate of γ; (d) the creation of new lymphocytes in the hosts' bone marrow and/or thymus with a rate of λ; and (e) the lymphocytes' natural death with a rate of σ.

Lymphocytes and pathogens obviously do not move in an empty space. Instead, they travel through the blood and the lymphatic system, but for the sake of simplicity, here we describe the movement of lymphocytes and pathogens as diffusion with rates D_y and D_x, respectively. Appropriate values for the rate constants in realistic systems are described in the Appendix.

Using these reactions, the ISP dynamics translates into a PP system. The deterministic continuous average description of this ISP model leads to the following ordinary differential equations (ODEs):

$$\frac{\partial x}{\partial t} = \alpha x - \gamma xy, \quad \frac{\partial y}{\partial t} = \lambda + \nu xy - \sigma y. \tag{1}$$

Two possible regimes are expected in the ODE solution of this system: (a) a stable zero-pathogen fixed point, where small perturbations decay rapidly to zero, and pathogens never manage to produce a full-blown infection, or (b) an unstable zero-pathogen fixed point, where the small perturbations converge to the positive fixed point, leading to the coexistence of the host immune system and the pathogen. These regimes do not seem to represent the experimental reality of pathogens growing and disappearing.

While the mean-field continuous description of this system fails to capture the proper dynamics, it can be used to understand the possible dynamical regimes emerging in the discrete stochastic realization of the same system. Specifically, the dynamics of the stochastic system depends on the fraction of time spent by the ODE solution near the zero-prey state. If this time is protracted, the stochastic aspect of the system can lead to an infection, followed by an extinction of the pathogen, or to a very slow, yet continuous, increase in the pathogen concentration, as is indeed observed [29,31,35,36].

Note that throughout this paper we consider the simplified model of Eq. (1). However, our conclusions can be generalized to most PP models. Such models are often represented by the

*louzouy@math.biu.ac.il

following set of equations

$$\frac{\partial x}{\partial t} = f_1(x) - g_1(x,y), \quad \frac{\partial y}{\partial t} = f_2(y) + g_2(x,y), \qquad (2)$$

where $f_1(x)$ and $f_2(y)$ represent the independent processes of birth, death, and competition within the predator and the prey populations in the absence of the other population. $g_1(x,y), g_2(x,y)$ are the interactions terms. The functions $f_1(x)$, $f_2(y)$, $g_1(x,y)$, and $g_2(x,y)$ considered are usually monotonic in x and y and satisfy $g_1(x,0) = g_1(0,y) = g_2(x,0) = g_2(0,y) = 0$, $f_1(0) = f_2(0) = 0$, $\forall x$, $\lim_{y\to\infty} g_1(x,y) - f_1(x) > 0$, and $\forall y$, $\lim_{x\to\infty}[f_2(y) + g_2(x,y)] > 0$ (except for the Holling-Tanner-type model [8–10]—for a review, see Refs. [18,37]). Within this description, the precise form of the system does not usually affect the number of fixed points. PP systems typically have two fixed points. If one of the points is stable or marginal, the second one is usually unstable. Note that in the case of the immune response, the predator (immune system cells) has a constant source term and is not annihilated in the absence of prey. The model studied here is obviously an extreme simplification of the immune response, but given its simplicity it produces a generic result that may be applicable to realistic situations.

Many aspects of deterministic and stochastic PP systems have been studied, but most models up to now have discussed the properties of the positive fixed points. The inclusion of spatial variability and diffusion in PP systems can have mixed effects. While in most of the systems diffusion was shown to stabilize the positive fixed point, in some systems it can have a strong destabilizing effect [9,14,38]. Diffusion can also stabilize the average behavior of a positive fixed point. Limited diffusion coupled with spatial heterogeneity prevents the stochastic transition to extinction through the infill of regions that become empty by flow from high-density regions of environment [9,15,18,39,40]. Other models have shown that predator-prey models can exhibit directed percolation [27] or Fisher waves [39,41], as is also observed here.

In a different context predator-prey systems were studied as excitable media by many groups [42–47]. Following the disappearance of the prey, the predator population decreases. However, often prey in different regions cannot reoccupy this region, since the predator population is still too high, leading to a "*de facto* refractory period."

Here we study a different aspect of PP dynamics by looking at the fluctuations near the zero fixed point of an ISP system with a constant source of immune cells, when the value of the positive fixed point is arbitrarily large. In discrete stochastic systems, the population of preys ultimately undergoes extinction. The extinction probability (at a finite time) starting from the positive fixed point decays exponentially with the number of predators and preys in the fixed point [23,40,48–52]. We study the transition to the absorbing state, following an escape from the same state. We show that, starting near the absorbing state, the dynamics of discrete stochastic spatially extended PP models is determined by three factors: the extinction probability of a small perturbation from the absorbing state in the discrete stochastic zero-dimensional PP model, the diffusion rate, and the system size. The interplay between these factors can lead to different dynamical regimes. These regimes are described in the following sections.

II. METHODS

A. ODE numerical solution

Equation (1) is nonstiff in the parameter regime studied, and was solved numerically using the ode45 MATLAB function, version 7.2.0.294 (R2006a), based on an explicit fourth-order Runge-Kutta formalism [53].

B. Monte Carlo simulations

Monte Carlo simulations were performed for the agent-based dynamics. The simulations were performed in one-, two-, and three-dimensional lattices by using a synchronous Poisson approximation of the mass-action dynamics. Specifically, at each iteration, the reaction rate of each reaction at each site was computed. The reaction was then enacted as a Poisson number added or removed with the appropriate average. Diffusion was only to first neighbors; the number of agents moving from one site to its neighbor was computed again using a Poisson distribution with a mean determined by the number of agents at the lattice site and the diffusion rate.

A precise description of the simulation can be found in previous publications [54–56]. In the absence of diffusion, the simulation results can be treated as an ensemble of zero-dimensional systems. The average of this ensemble is the averaged zero-dimensional stochastic counterpart of the mean-field results. In all simulations, the reactant concentrations were initiated in each lattice point at (x_i, y_0) with $x_i = 3$ (much lower than the positive fixed-point pathogen population). The reactions and diffusion were discrete and implemented separately according to the probabilities computed at each lattice point. The lattices sizes were 10 000, 100×100, and $22 \times 22 \times 22$, for one, two, and three dimensions, respectively.

C. Directed percolation analysis

Directed percolation [57] (DP) is a model for the spreading of a substance in a lattice in discrete time steps. Each lattice point can have a value of zero or one, and lattice points with values of one can invade a neighboring point. The fraction of lattice points with values of one is determined by the ratio between the invasion probability and the extinction probability at each site. If this value is higher than a percolation threshold, the lattice occupancy (the fraction of lattice points that have a value of one) will be positive at finite times, while below this value, it will be null. The transition between two states is a second-order phase transition [58]. In the current realization, we compared the extinction and invasion rate of the DP description with the pathogen disappearance probability and diffusion in the full ISP model. At each time step, the value at a given lattice point was computed based on its own value, and the values of its first neighbors in the previous step (2 in 1D, 4 in 2D, and 6 in 3D simulations). First, a disappearance probability $p(\text{dis}) = p: 1 \to 0$ was applied to each lattice point with a value of 1. Then a probability of diffusion $p(\text{inv}) = p: 0 \to 1$ was applied from each lattice point that had a value of 1 in the previous time step to its nearest neighbors. The lattice sizes used in 1D, 2D, and 3D were 10 000, 100×100, and $22 \times 22 \times 22$, respectively. The

simulations were initiated with the entire lattice set to 1. The directed percolation results presented in Fig. 6 were computed after 500 time steps, and are an average over 50 simulations for each set of parameters.

D. Critical exponents near DP threshold

In order to study the survival-extinction transition phase of the system, critical exponents near the percolation thresholds were computed in 1+1 and 2+1 dimensions. We computed the following parameters: (a) The density of active sites $\rho(t) \sim t^{-\delta}$ is associated with dynamical critical exponent δ; (b) the stationary density of active sites $\rho^{\text{stat}} \sim (p - p_c)^{\beta}$ is computed in the supercritical phase and is associated with the critical exponent β; and (c) the temporal length scale $\xi_{\|} \approx |p - p_c|^{-\nu_{\|}}$ associated with critical exponent $\nu_{\|}$ was calculated in the subcritical phase.

We used a two-dimensional lattice of size 100×100 and a one-dimnesional lattice with 500 lattice sites. We then ran the Monte Carlo simulations with the parameters $\alpha = 1.2$, $\gamma = 0.2$, $\lambda = 0.6$, $\nu = 0.08$, $\sigma = 0.58$, and $D_y = 0.025$ for different values of D_x. For each value of D_x, 100 realizations of the simulations with the same initial-state conditions were done. The initial state ($t = 0$) is defined by the lattice fully occupied by preys ($x_i = 3$ for each lattice site i) and Poisson-distributed predators with a mean of 1. The number of nonempty lattice sites was calculated for each realization after $t = 250$ and the density of active sites was computed as an ensemble average. For the analysis of the temporal length scale, the time of the population extinction was calculated for each realization, and averaged over all realizations for each value of D_x. The percolation threshold was calculated to within an accuracy of $\pm 0.000\,05$. The exponents were calculated as the best linear fit of $\rho(t)$, ρ^{stat}, and $\xi_{\|}$ functions in a double-logarithmic scale.

III. RESULTS

A. Mean-field approximation

The mean-field dynamics of the ISP model studied here are defined by Eq. (1). This model is an extension of the classical LV PP model, with a nonzero-predator basal concentration.

Equation (1) has two fixed points, only one of which is stable. If $\alpha > \lambda\gamma/\sigma$, the $(0,\lambda/\sigma)$ fixed point is unstable, and the $[(\sigma - \lambda\gamma/\alpha)/\upsilon,\alpha/\gamma]$ is stable. The opposite occurs if $\alpha < \lambda\gamma/\sigma$. In this case, the unstable fixed point is actually in the nonbiological regime of negative predator density. Let us denote the zero and positive fixed points by $(0, y_0)$ and (x^*, y^*), respectively. In the zero-dimensional discrete stochastic realization of such a system, when x^* is low, the system can first converge to its stable attractor (x^*, y^*) and then jump to the absorbing state $(0, y_0)$. Note that in such a case, the stochasticity is only due to the discrete nature of the reactants and no external noise is assumed. The transition to the absorbing state occurs as a result of the discrete nature of the pathogen [59]. Such transitions have been extensively studied in other contexts [4,8–10,13,15,18,23,37,40,50,51,60–64]. When this is the mechanism of extinction, the convergence time to the absorbing state grows exponentially with the number of predators and preys in the positive fixed point [26,60,65,66]. Thus, in finite systems and finite times, the transition probability to the absorbing state is expected to vanish for large values of (x^*, y^*).

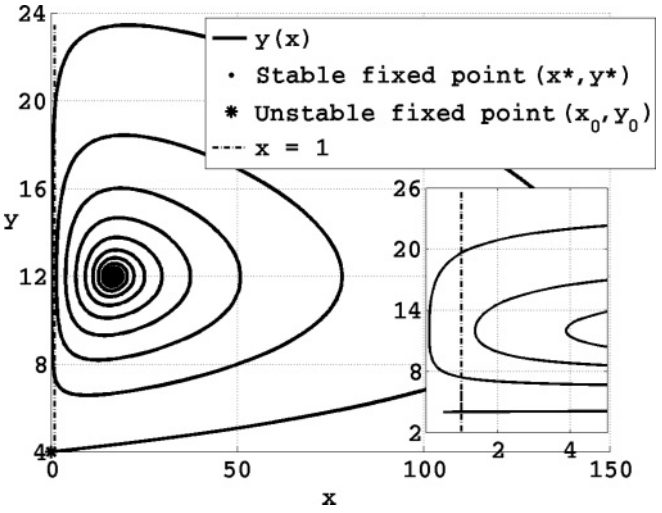

FIG. 1. Trajectories of the ODE solution of immune system-pathogen dynamics. The trajectories start from a point near the zero-pathogen fixed point and oscillate toward the positive fixed point. At each oscillation, the trajectories are getting farther away from the y axis. During the first oscillations, the trajectories can stay for a long time in a region where the expected pathogen population is less than 1. In this region there is a high pathogen disappearance probability (inset). The parameters used for these results are $\alpha = 1.2$, $\gamma = 0.1$, $\lambda = 0.4$, $\nu = 0.004$, $\sigma = 0.1$, $D_x = D_y = 0$, and $t = 200$.

Here we study a different mechanism of extinction occurring when the fixed point (x^*, y^*) is stable and the values of (x^*, y^*) are high. In such a case, the course of a disease can be represented as a perturbation of the unstable $(0, y_0)$ fixed point.

In the zero-dimensional discrete system, there is a large region in parameter space where the system converges to the absorbing state. Starting from a small perturbation near $(0, y_0)$, the transition to the absorbing state for high values of (x^*, y^*) occurs most probably during the first pass near the zero-pathogen state (Fig. 1). Note that if the initial perturbation is too small, there is also a non-negligible probability that the system will directly converge to the absorbing state. Here we assume that the initial perturbation is large enough and that this effect is secondary. The probability of moving to the absorbing state at the first pass near zero increases with the time spent at the low pathogen value. Let us denote the pathogen extinction probability as $P^{\text{local}}_{\text{disappearance}}$. $P^{\text{local}}_{\text{disappearance}}$ can be roughly approximated by simplifying the dynamics in the range of low x values. In order for the pathogen to disappear, it must pass through the $x = 1$ state. Assume that $x = 1$ is obtained for a given value $\tilde{y}$ of y. The stochastic dynamics of y can be approximated by their deterministic mean-field model $y\prime = \lambda - \sigma y$. We ignore the $+\upsilon x y$ term, since x is very small. The pathogen population x is low (or zero) as long as $y > \alpha/\gamma$. If the pathogen population does not vanish by the time $y \approx \alpha/\gamma$, it will start growing again. The time it takes for y to reach this value is approximately $\Delta t_1 = \frac{1}{\sigma} \ln[(\tilde{y} - \frac{\lambda}{\sigma})/(\frac{\alpha}{\gamma} - \frac{\lambda}{\sigma})]$. Even when the pathogen population starts growing, it still can be eradicated. The probability of pathogen eradication practically vanishes when the expected value of x is larger than 1. Note that the y population has a constant source term

and its trajectories do not pass near zero. We thus ignore the effect of possible stochastic effects on the y population.

Once y is small compared to α/γ, its effect on the expected value of x can be ignored. The time it takes for x to increase from 1 to a larger number (say, k) is thus $\Delta t_2 = \frac{1}{\alpha}\ln k$. During the time interval $\Delta t_1 + \Delta t_2$, the x population has a disappearance probability of $\gamma y \Delta t$ per unit time Δt. Its survival probability is thus $1 - \gamma y \Delta t$ and the cumulative survival probability can be approximated by

$$\Pi(1 - \gamma y \Delta t) = e^{\sum \ln(1-\gamma y \Delta t)} \approx e^{-\gamma \int y dt}.$$

One can thus use the previous computation of the time interval $\Delta t_1 + \Delta t_2$ to estimate the disappearance probability in a given pass near the zero-pathogen state as

$$P^{\text{local}}_{\text{disappearance}} = P(\text{disappearance}|\tilde{y}_0) = 1 - e^{-\gamma \int_{\Delta t_1 + \Delta t_2} y dt}.$$

Another analysis of the disappearance probability in a slightly different system has been recently developed by Meerson *et al.* [67]. The convergence probability to the zero-pathogen absorbing state increases with a value of (x^*, y^*) in both simulations (Fig. 2) and the above approximation. The disappearance of the pathogens in this system is thus not due to low values of x at the fixed point. It occurs following transient low values on the trajectory to the fixed point. For constant initial conditions, as the values of x^* and y^* increase, the trajectory will pass closer to the y axis (as can be easily seen from a geometrical perspective), and the pathogen disappearance probability in the first pass near zero increases. Equations (1) and their stochastic zero-dimensional counterpart (see Sec. II) were solved numerically for different values of (x^*, y^*). For each value of (x^*, y^*), the fraction of stochastic realizations ending at the absorbing state was computed (Fig. 2). The observed transition to the absorbing state does not result from the low total number of agents in the simulation, but from the large distance between the starting conditions and the positive fixed point.

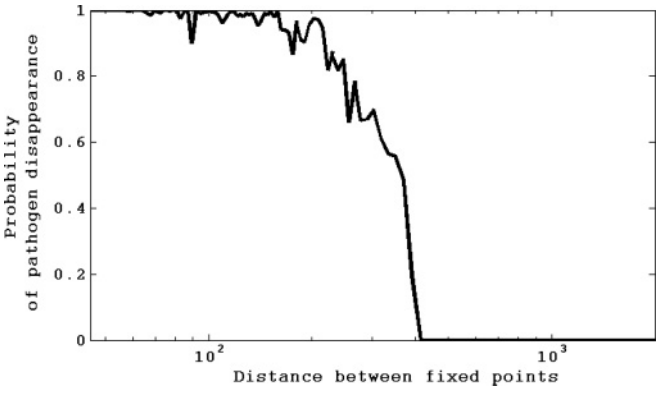

FIG. 2. Probability of pathogen disappearance as a function of distance between fixed points. The pathogen disappearance probability (at the first pass near zero) grows with the distance between the zero-pathogen fixed point and the positive fixed point. The parameters used in this figure are $\alpha = 1.2$, $\gamma = 0.1$, $\lambda = 0.4$, $\sigma = 0.1$, and ν runs from 10^{-5} to 1.5×10^{-3}. The distance between the fixed points is defined as the Euclidean distance.

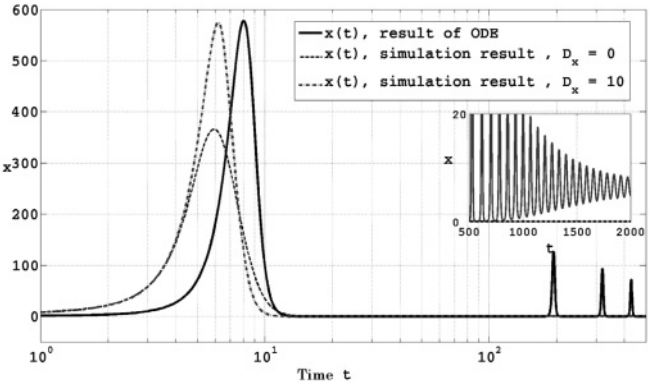

FIG. 3. Simulations with high disappearance probabilities. Pathogen average population as a function of time for the ODE solution (solid line), the $D_x = 0$ stochastic simulation (dashed line), and the $D_x = 10$ stochastic simulation (dotted-dashed line). Both the low and high diffusion rate simulations converge to the nonstable zero-pathogen state in contrast with the mean-field ODE. The parameters used for these results are $\alpha = 1.6$, $\gamma = 0.01$, $\lambda = 0.6$, $\nu = 0.001$, and $\sigma = 0.01$.

Thus, the apparent discrepancy between the observed pathogen rise and extinction and the predictions of the deterministic continuous PP system can be simply explained by using the transition of the trajectory very close to the y axis. In other words, at some stage the pathogen number is so low that it shrinks to zero (Fig. 3).

B. Spatially inhomogeneous dynamics

The effect on $P^{\text{local}}_{\text{disappearance}}$ of moving to higher dimensions is different for large and small values. If $P^{\text{local}}_{\text{disappearance}}$ is low, diffusion stabilizes the positive fixed point (data not shown), as often happens in PP systems [9,14,38]. Here we are interested in the opposite regime where $P^{\text{local}}_{\text{disappearance}}$ is almost 1.

Assume $P^{\text{local}}_{\text{disappearance}}$ is high enough such that the survival probability in one pass near the y axis even in a single spot in the entire system is low. In such a case, the positive fixed point is never obtained in the absence of diffusion. If the diffusion is zero, each region in turn will be absorbed to the zero-pathogen state until the entire system will converge to the absorbing state after a single pass near zero. The transition to extinction occurs since regions with no pathogens cannot be colonized by regions where the pathogen concentration is still finite. If the diffusion rate is too high, the system behaves as the mean field and all pathogens die simultaneously as the local pathogen density becomes too low. Thus, if $P^{\text{local}}_{\text{disappearance}}$ is high and the diffusion rate is either very low or very high, the pathogen population will disappear (Fig. 4). In intermediate ranges of diffusion rates, colonization can take place and complex dynamics can emerge from a combination of asynchronous pathogen dynamics and high diffusion rates. Interestingly, within this parameter range, the transition between the two regimes is determined by the system size, and not only by the values of the rate constants.

C. Directed percolation

At high values of $P^{\text{local}}_{\text{disappearance}}$ and intermediate diffusion rates, an interesting invasive regime emerges. Independently,

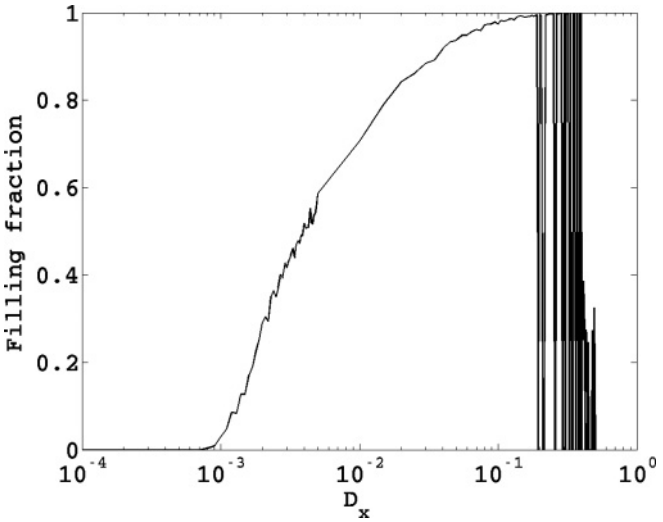

FIG. 4. Pathogen filling fraction as a function of diffusion rate. The stochastic simulations results in 2D ($d = 2$). The lattice size is 100×100. The parameters used for this figure are $\alpha = 1.6$, $\gamma = 0.1$, $\lambda = 0.4$, $\nu = 0.004$, $\sigma = 0.1$, and $2dD_y = 0.01$. For low and high values of pathogen diffusion rates, the pathogen population becomes extinct. For high values of D_x, there are rare events of population survival. The number of such events decreases as D_x grows. Note that the curve is nonsymmetric. For low diffusion rates, a part of the space is occupied, while for a high diffusion rate either all or nothing is occupied. The filling fraction is defined as the fraction of lattice points with nonzero-pathogen values.

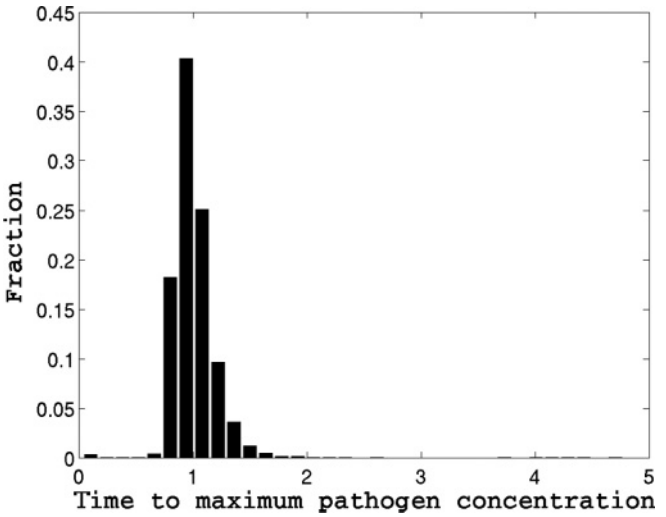

FIG. 5. Distribution of times to the maximal pathogen population in different realizations of the same system. All realizations were started with equal initial conditions. The units are the fraction of the expected time in the ODE realization of the system. The time to maximum pathogen concentration was measured in the first oscillation. One can clearly see a large distribution of times even for the first oscillations. The variance results from the first few interactions occurring at low pathogen and immune system cell numbers.

at each position, the low number of pathogens in the initial condition leads to stochastic variations in the time at which the pathogen population is minimal and to a loss of synchronization (Fig. 5). Thus, by the time the pathogen population in a given site is annihilated, neighboring sites may still have a nonzero-pathogen population. In such a case, if the diffusion rate is high enough, the pathogen in the neighboring sites can colonize the empty site, once the immune system cell concentration is low enough in the colonized site. Following this invasion, the pathogen population can rise again.

Such a dynamics appears to be similar to a directed percolation (DP) model. DP is a lattice model with two possible reactions: invasion of a neighboring site and extinction in a site [68,69]. DP systems show a second-order phase transition at a critical filling fraction. Below this filling fraction, after a long enough finite time, the system will be empty, while above it, large enough systems will still contain connected system size clusters of active sites [58]. The presence of the DP regime in predator-prey models was derived in some previous studies [23,70–73]. The fraction of space with a nonzero-pathogen population was measured in Monte Carlo simulations of the ISP model in 1D, 2D, and 3D for different values of D_x and $P^{\text{local}}_{\text{disappearance}}$. We then compared these results to simulations of a DP model with parallel invasion and extinction rates (see Sec. II). In the DP model, each lattice site was assigned a value of either zero or one. Each lattice site with a value of one could become zero with a probability of $p(\text{dis})$ and it could invade neighboring sites with a probability of $p(\text{inv})$. The system was initiated with a fully occupied lattice. We run this simulation for different values of $p(\text{dis})$ and $p(\text{inv})$, and run in parallel simulations of the full ISP with $p(\text{dis}) = P^{\text{local}}_{\text{disappearance}}$ and $p(\text{inv}) = D_x$ (Fig. 6). After the system converged to its steady-state filling fraction, we measured the filling fraction as a function of $p(\text{inv})$. The percolation transition in 2D and 3D is in good agreement with the full ISP dynamics Monte Carlo simulation (Fig. 6). However, in the 1D system, the fit is limited. The finite pathogen concentration in this regime results from an amalgam of regions where the pathogen population has vanished and regions have been recolonized by the pathogen (data not shown). To summarize, if the diffusion rate is intermediate and $P^{\text{local}}_{\text{disappearance}}$ is high, the dynamics can be explained by a simple DP process that is only determined by $p(\text{dis})$ and $p(\text{inv})$, *at least in 2D and 3D*. In 1D, the precise dynamics of the DP and the full ISP only agrees qualitatively.

In order to validate that the ISP system can be modeled as a directed percolation, we computed some critical exponents for a two-dimensional ISP system (see Table I and Fig. 7 for some of the exponents). As can be clearly seen, in 2D, the exponents of the full ISP are in good agreement, while in 1D, even the β exponent (the fraction of space occupied) does not fit the DP model. This is in agreement with the results obtained for the fit between the DP and the full ISP model.

TABLE I. Estimates for critical exponents of ISP model and directed percolation obtained by numerical methods. In 2D, the exponents of the full ISP are in good agreement, while in 1D, even the β exponent (the fraction of space occupied) does not fit the DP model.

Dimension	ISP-2d	d = 2 + 1	ISP-1d	d = 1 + 1
β	0.54	0.58	0.5	0.276
δ	0.44	0.45	0.24	0.16
$\nu_{\parallel}$	1.23	1.29	1.4	1.73

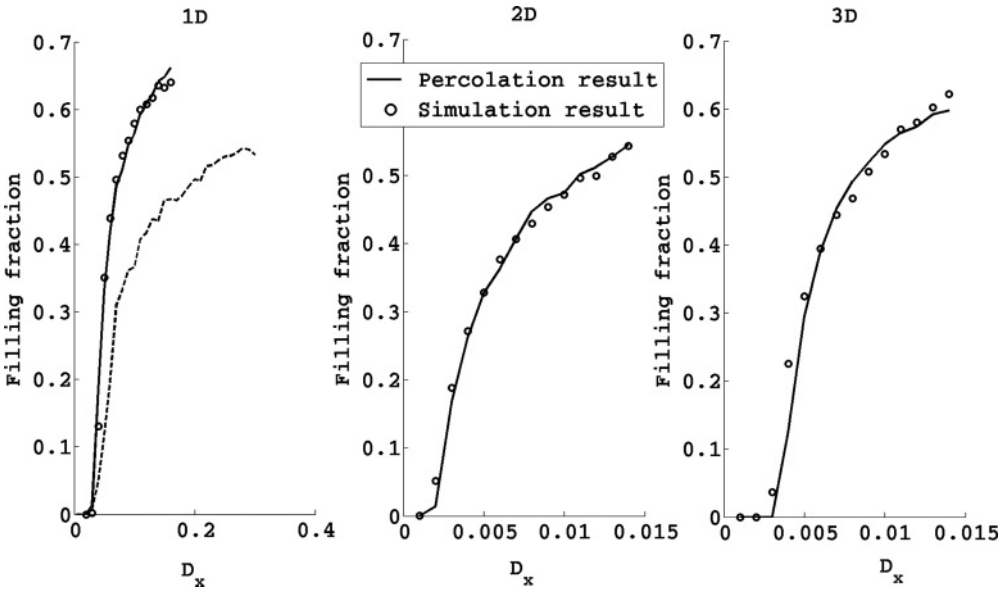

FIG. 6. Percolation results and a comparison to filling fraction. The solid line is the percolation transition in the DP model [lattice filling fraction vs p(inv)], which is in good agreement with the full ISP simulation results (scatter plot) (lattice filling fraction vs D_x). For the 2D and 3D systems, the Monte Carlo simulation and DP simulation results coincide for $p(\text{inv}) = P^{\text{local}}_{\text{disappearance}} = 0.35$. In the 1D case, the diffusion itself affects $P^{\text{local}}_{\text{disappearance}}$, yielding an effective $P^{\text{local}}_{\text{disappearance}}$ of 0.19. The parameters used in the Monte Carlo simulation are $\alpha = 1.2$, $\gamma = 0.2$, $\lambda = 0.6$, $\nu = 0.08$, and $\sigma = 0.58$.

D. Wave trains

In parallel to the DP regime, a different behavior can emerge in the same parameter range. For most simulation trials, the pathogen population follows a DP dynamics. There are, however, rare events where in one lattice point the pathogen population does not disappear in multiple passes near zero. In each following pass, the disappearance probability decreases until it is negligible. This point can then convert nearby points to a stable fixed point through the propagation of Fisher waves [74], until the entire space converges to the positive fixed point. The Fisher waves advance with a linear rate, and the filling fraction (the fraction of space with nonzero-pathogen population values) grows proportionally to the dimension of the system (see, for example, a quadratic growth in a 2D system in Fig. 8). A similar process was observed when computing the dynamics of a predator and a prey occupying a new territory [75,76], and this is called wave trains when the central point is marginally stable.

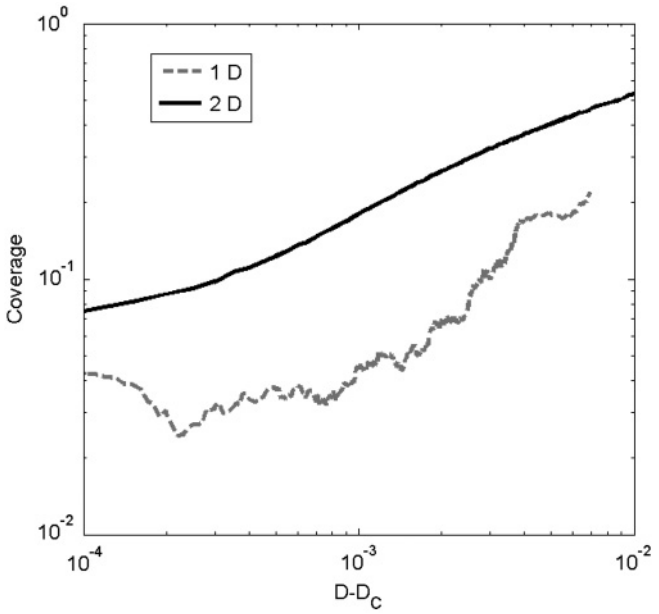

FIG. 7. Parameters of critical behavior. Estimate of the β critical exponents through the coverage fraction (the density of active sites) $\rho(t)$ as a function of time obtained for $D_x = 0.006\,85$, which corresponds to $\delta = 0.4421$ in a 2D system and for $D_x = 0.0382$ in 1D. Note that the 1D system is much noisier than the 2D system.

Since $P^{\text{local}}_{\text{disappearance}}$ is finite, there is a chance in any system that has not converged to the zero-pathogen state in the entire system to converge locally to the wave-train regime. Following the local convergence, the entire system will eventually attain the positive fixed-point value. The only mechanism limiting the transition to the wave-train regime and following it to the stable fixed point is the transition to the absorbing state. The transition probability to the absorbing state in the directed percolation regime is inversely proportional to the exponent of the system size [58]. At any given time, the transition probability to the wave-train regime is linearly proportional to the system size. Thus as the system grows, at finite times, there is a higher probability of transition to the wave-train regime and a lower probability of transition to the absorbing state (Fig. 9). Note that for any system size, the system will always eventually converge to the absorbing state, but the transition rate to extinction may be exponentially small.

E. Synchronization

As mentioned before, a third possible, albeit less interesting, dynamical regime is full synchronization. In the system

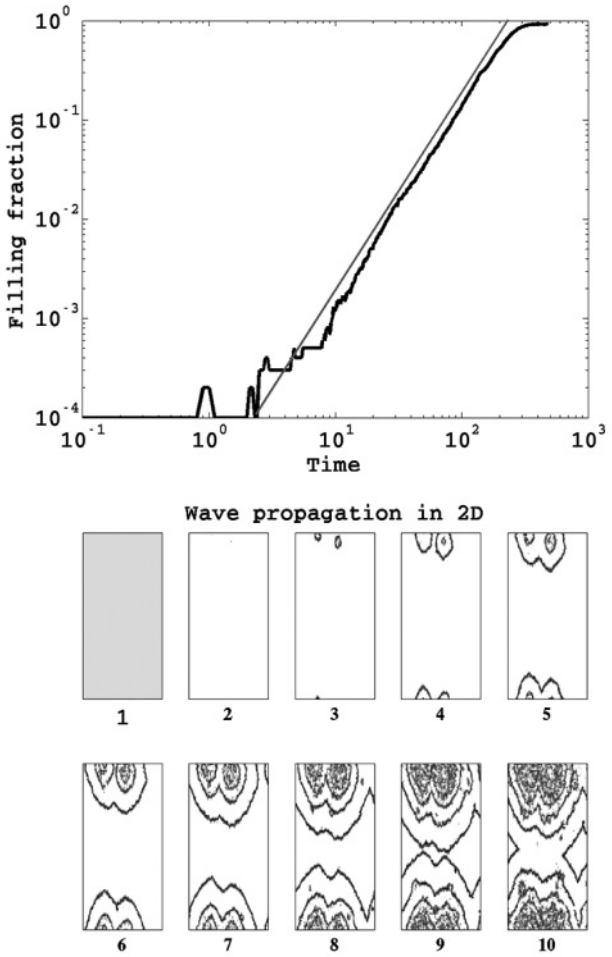

FIG. 8. Wave-train dynamics. The upper drawing represents the pathogen filling fraction, which is a quadratic function of time, since the wave front advances at a linear rate in a 2D space. The thin gray line is a line representing $y = t^2$. The lower drawing represents the wave creation and propagation in space-time. The first snapshot refers to the uniform filling of the 2D space by pathogens. In the second snapshot, the pathogen extinction can be observed in all but two of the pixels. These two pixels are the source of the following wave that is seen propagating in the next snapshots. The tenth snapshot shows the population survival following the wave filling the 2D space.

studied here, the DP dynamics is the direct result of the loss of synchronization among patches. If all regions oscillate synchronously, the entire system will converge to the zero-pathogen state. Beyond some diffusion rate, all patches are synchronous. The system then behaves as in the mean field (Fig. 3) and extinction occurs at the first pass near zero. Note that in such a system the total pathogen concentration even at a minimal value before the collapse can be very high. The limiting factor is the local concentration, not the global one. Thus in the human body where diffusion may be high, the fate of pathogens may be significantly affected by the diffusion rate, and different regimes may be linked to different diffusion rates.

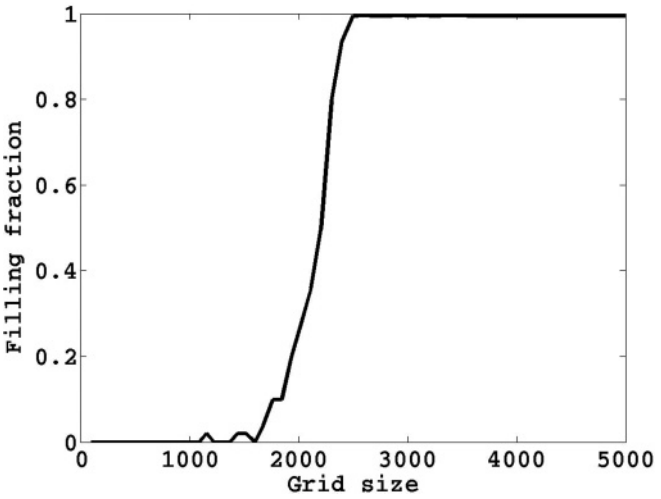

FIG. 9. Effect of system size on survival probability. The ISP simulations were run with the same parameters ($\alpha = 1.6$, $\gamma = 0.1$, $\lambda = 0.4$, $\nu = 0.004$, $\sigma = 0.1$, $2dD_x = 0.8$, and $2dD_y = 0.01$) for different 2D system sizes, ranging from 10×10 to 150×150. For each system size 50 realizations were done and the average fraction of nonempty sites was calculated. The filling fraction rises sharply as the system size passes $1/P^{\text{local}}_{\text{disappearance}}$, until it saturates on 1 in systems significantly larger than that.

IV. DISCUSSION

Here we have studied an extension of the predator-prey model to the interaction between the immune system and pathogens. This system has two fixed points, only one of which has a positive pathogen concentration. The ODE solution of perturbations around the zero-pathogen fixed point leads to two possible scenarios: either the perturbation collapses directly back to the zero-pathogen fixed point or it cycles toward the positive pathogen concentration fixed point. Both scenarios are in contrast with the observed immunological reality, where the pathogen population usually first rises and then converges back to zero.

This apparent discrepancy can be solved by the inclusion of stochastic discrete pathogens. If the positive fixed point has high enough pathogen and immune system cell concentrations, any small perturbation will first grow and then converge to the absorbing state, which is the counterpart of an unstable fixed point in the ODE description.

When stochasticity, diffusion, and spatial heterogeneity are introduced into the system, three scenarios can emerge: (a) the ODE solution; (b) a directed percolation regime, where regions with no pathogens are reoccupied by pathogens from neighboring points; and (c) Fisher waves (wave trains).

The transition probabilities between the regimes are affected by three elements: the probability of pathogen disappearance following a pass near the zero-pathogen state, the diffusion rate, and the system size. As the system grows, the pathogen survival probability increases. Beyond these elements, these results are not sensitive to the precise details of the PP model or to the precise structure of space used. We have previously shown a similar conclusion in a very different system of catalyst-induced growth [77].

This system has another interesting aspect. Grassberger and Janssen [69,78] proposed that under a set of limiting conditions, many dynamical systems belong to the DP universality class. Only recently was the experimental validation of directed percolation found in (2+1) dimensions [79]. However, altogether, and to the best of our knowledge, there are very few known two-variable systems with DP behavior. We have previously proposed a catalyst-induced growth system as a prototype of such systems [54], but in that system the percolation was mainly from one catalyst to the other and the substrate was just used to define a spatiotemporal scale of the link between catalysts. Our work here attempts to provide an example of DP dynamics in a more realistic two-variable system.

We have also previously studied the relation of PP systems with Fisher waves in the context of human immunodeficiency virus (HIV) dynamics [80]. This was done in the context of a local seeding of the pathogen, and the expansion of the zone where the stable fixed point was attained. The currently proposed model shows that a similar regime can emerge even if the pathogen is seeded uniformly.

APPENDIX: APPROPRIATE PARAMETER VALUES FOR ISP MODEL

Since the model is designed to describe the dynamics of many different infections, both acute and chronic, it is almost impossible to provide one set of parameters that would be appropriate for different infections. It is clear that many parameters will be different for different infections. We nevertheless discuss constraints on the parameter values used in our simulations to limit the parameter range to be checked. Note that these limits do not limit the validity of the dynamical regimes studied here. We use influenza as an example of an acute infection:

$$\frac{\partial x}{\partial t} = \alpha x - \gamma xy, \quad \frac{\partial y}{\partial t} = \lambda + vxy - \sigma y.$$

For several viral infections, such as HIV, hepatitis C virus (HCV), and influenza (in mice), viral particles have been found to be very short lived with $c = 6 - 25\ \text{day}^{-1}$ [81,82]. The death rate of infected cells is likely to vary substantially depending on whether the virus is cytopathic or not. In an HIV-1 infection, it is 0.5–1 day^{-1} [83,84], while in an influenza infection of mice it is 0.7–1.6 day^{-1} [82], leading to the destruction of infected cells that has an order of 1 per day. However, this is the total level that is affected by the amount of T cells killing these infected cells. Killing of infected cells by the cytotoxic T lymphocyte (CTL) response occurs at a per capita rate (γ) of $2 \times 10^{-5}\ \text{day}^{-1}\,\text{cell}^{-1}$ [85–88]. During viral infections, the population of CTLs expands at a rate of 0.5–2 day^{-1} [87,89–92]. Thus the peak values of vx should be set to an order of 1. The death rate of effectors after the peak (σ) has been estimated to be 0.1–0.4 day^{-1} [91,93]. The basal production rate of target-specific immune system clones (λ) is unknown. However, current estimates of the number of such clones range at the 10^6 clone level [94] and the turnover of such cells is of the orders of hundreds of days. We can thus assume that practically every clone is randomly created many times every day, and we can thus set λ to be higher than all other variables. The value of α is determined by the product of the virus infectivity and production rate. It is chosen such that the rate of increase in the virus population over time is in the range 0.1–5 day^{-1}, as has been observed in HIV and influenza infection [82,95,96].

[1] A. J. Lotka, *Elements of Physical Biology* (Williams & Wilkins, Baltimore, MD, 1925).
[2] A. J. Lotka, J. Am. Chem. Soc. **42**, 1595 (1920).
[3] A. J. Lotka, Proc. Natl. Acad. Sci. USA **8**, 147 (1922).
[4] V. Volterra, Mem. Acad. Lincei **2**, 31 (1926).
[5] A. A. Berryman, Ecology **73**, 1530 (1992).
[6] G. F. Gause, Science **79**, 16 (1934).
[7] R. Arditi and L. R. Ginzburg, J. Theor. Biol. **139**, 311 (1989).
[8] J. D. Murray, *Mathematical Biology* (Springer-Verlag, New York, 1989).
[9] Yihong Du and S.-B. Hsu, J. Differential Equations **203**, 331 (2004).
[10] A. R. Ives, B. J. Cardinale, and W. E. Snyder, Ecol. Lett. **8**, 102 (2005).
[11] A. J. Nicholson and V. A. Bailey, Proc. Zool. Soc. London Part 1 **3**, 551 (1935).
[12] M. L. Rosenzweig, Science **171**, 385 (1971).
[13] H. I. Freedman and G. S. K. Wolkowicz, Bull. Math. Biol. **48**, 493 (1986).
[14] M. G. Neubert, M. Kot, and M. A. Lewis, Theor. Popul. Biol. **48**, 7 (1995).
[15] H. I. Freedman and Y. Takeuchi, Applicable Anal. **31**, 247 (1989).
[16] A. M. de Roos, E. McCauley, and W. G. Wilson, Theor. Popul. Biol. **53**, 108 (1998).
[17] G. Yaari, S. Solomon, M. Schiffer, and N. M. Shnerb, Physica D **237**, 2553 (2008).
[18] C. J. Briggs and M. F. Hoopes, Theor. Popul. Biol. **65**, 299 (2004).
[19] P. H. Leslie and J. C. Gower, Biometrika **47**, 219 (1960).
[20] U. Dobramysl and U. C. Täuber, Phys. Rev. Lett. **101**, 258102 (2008).
[21] G. Q. Cai and Y. K. Lin, Ecol. Complexity **4**, 242 (2007).
[22] R. Law, M. J. Plank, A. James, and J. L. Blanchard, Ecology **90**, 802 (2009).
[23] M. Mobilia, I. T. Georgiev, and U. C. Täuber, Phys. Rev. E **73**, 040903 (2006).
[24] K. C. de Carvalho and T. Tome, Int. J. Mod. Phys. C **17**, 1647 (2006).
[25] U. Dieckmann, P. Marrow, and R. Law, J. Theor. Biol. **176**, 91 (1995).
[26] M. J. Washenberger, M. Mobilia, and U. C. Täuber, J. Phys. **19**, 65139 (2007).
[27] M. Mobilia, I. T. Georgiev, and U. C. Täuber, e-print arXiv:q-bio/060939v1.
[28] A. K. Abbas and A. H. Lichtman, *Cellular and Molecular Immunology*, 5th ed. (Saunders/Elsevier Science, Philadelphia, 2003).

[29] C. A. Janeway Jr., P. Travers, M. Walport, and M. J. Shlomchik, *Immunobiology. The Immune System in Health and Disease*, 6th ed. (Garland Science, New York, 2005).

[30] K. P. Murphy, P. Travers, M. Walport, C. Janeway, M. Ehrenstein, and C. Mauri, *Janeway's Immunobiology* (Garland, New York, 2007).

[31] D. H. Busch and E. G. Pamer, Immunol. Lett. **65**, 93 (1999).

[32] M. F. Bachmann, B. Odermatt, H. Hengartner, and R. M. Zinkernagel, J. Exp. Med. **183**, 2259 (1996).

[33] M. Rambeaud, R. A. Almeida, G. M. Pighetti, and S. P. Oliver, Vet. Immunol. Immunopathol. **96**, 193 (2003).

[34] M. Schaeffer, S. J. Han, T. Chtanova, G. G. van Dooren, P. Herzmark, Y. Chen, B. Roysam, B. Striepen, and E. A. Robey, J. Immunol. **182**, 6379 (2009).

[35] M. P. Busch and G. A. Satten, Am. J. Med. **102**, 117 (1997).

[36] E. G. Pamer, Nat. Rev. Immunol. **4**, 812 (2004).

[37] A. D. Taylor, Ecology **71**, 429 (1990).

[38] A. Hastings, J. Math. Biol. **5**, 399 (1977).

[39] W. S. Gurney and A. R. Veitch, Bull. Math. Biol. **62**, 61 (2000).

[40] M. G. Neubert and M. Kot, Math. Biosci. **110**, 45 (1992).

[41] W. Gurney, A. Veitch, I. Cruickshank, and G. McGeachin, Ecology **79**, 2516 (1998).

[42] M. Banerjee and S. Petrovskii, Theor. Ecol. **4**, 37 (2011).

[43] J. Truscott and J. Brindley, Bull. Math. Biol. **56**, 981 (1994).

[44] V. Biktashev, J. Brindley, A. Holden, and M. Tsyganov, e-print arXiv:nlin/0406012.

[45] H. Malchow, F. Hilker, R. Sarkar, and K. Brauer, Math. Comput. Modell. **42**, 1035 (2005).

[46] E. Zemskov and A. Y. Loskutov, J. Exp. Theor. Phys. **107**, 344 (2008).

[47] M. A. Tsyganov, J. Brindley, A. V. Holden, and V. N. Biktashev, Phys. Rev. Lett. **91**, 218102 (2003).

[48] A. F. Rozenfeld, C. J. Tessone, E. Albano, and H. S. Wio, Phys. Lett. A **280**, 45 (2001).

[49] U. Dieckmann and R. Law, J. Math. Biol. **34**, 579 (1996).

[50] G. Domokos and I. Scheuring, J. Theor. Biol. **227**, 535 (2004).

[51] R. Rudnicki and K. Pichor, Math. Biosci. **206**, 108 (2007).

[52] B. A. Reid, U. C. Täuber, and J. C. Brunson, Phys. Rev. E **68**, 046121 (2003).

[53] K. E. Atkinson, *An Introduction to Numerical Analysis* (Wiley India, New Delhi, 2008).

[54] A. Agranovich, Y. Louzoun, N. Shnerb, and S. Moalem, J. Theor. Biol. **241**, 307 (2006).

[55] Y. Louzoun, S. Solomon, H. Atlan, and I. R. Cohen, Bull. Math. Biol. **65**, 375 (2003).

[56] N. M. Shnerb, Y. Louzoun, E. Bettelheim, and S. Solomon, Proc. Natl. Acad. Sci. USA **97**, 10322 (2000).

[57] S. R. Broadbent and J. M. Hammersley (unpublished).

[58] H. Hinrichsen, Adv. Phys. **49**, 815 (2000).

[59] V. Elgart and A. Kamenev, Phys. Rev. E **70**, 041106 (2004).

[60] M. Mobilia, I. T. Georgiev, and U. C. Täuber, J. Stat. Phys. **128**, 447 (2007).

[61] N. M. Shnerb, E. Bettelheim, Y. Louzoun, O. Agam, and S. Solomon, Phys. Rev. E **63**, 021103 (2001).

[62] R. M. Anderson and R. M. May, Philos. Trans. R. Soc., B **314**, 533 (1986).

[63] R. Arditi, J. M. Callois, Y. Tyutyunov, and C. Jost, C. R. Biol. **327**, 1037 (2004).

[64] J. Cardy and U. C. Täuber, Phys. Rev. Lett. **77**, 4780 (1996).

[65] R. Abta and N. M. Shnerb, Phys. Rev. E **75**, 051914 (2007).

[66] U. C. Täuber, in *Encyclopedia of Complexity and Systems Science*, edited by R. A. Meyers (Springer, New York, 2009), p. 3360–3374.

[67] B. Meerson and P. V. Sasorov, Phys. Rev. E **80**, 041130 (2009).

[68] P. Grassberger and A. De La Torre, Ann. Phys. **122**, 373 (1979).

[69] P. Grassberger, J. Phys. A **22**, 3673 (1989).

[70] E. Arashiro and T. Tome, J. Phys. A **40**, 887 (2007).

[71] L. Rodrigues and T. Tome, Braz. J. Phys. **38**, 87 (2008).

[72] T. Tome and R. M. Ziff, Phys Rev. E **82**, 051921 (2010).

[73] J. Wendykier, A. Lipowski, and A. L. Ferreira, Phys Rev. E **83**, 031904 (2011).

[74] R. A. Fisher, Ann. Eugen. **7**, 355 (1937).

[75] J. A. Sherratt, Physica D **117**, 145 (1998).

[76] J. A. Sherratt and M. J. Smith, J. R. Soc., Interface **5**, 483 (2008).

[77] Y. Louzoun, N. M. Shnerb, and S. Solomon, Eur. Phys. J. B **56**, 141 (2007).

[78] H. K. Janssen, Z. Phys. B **42**, 151 (1981).

[79] K. A. Takeuchi, M. Kuroda, H. Chate, and M. Sano, Phys. Rev. Lett. **99**, 234503 (2007).

[80] U. Hershberg, Y. Louzoun, H. Atlan, and S. Solomon, Physica A **289**, 178 (2001).

[81] B. Ramratnam, S. Bonhoeffer, J. Binley, A. Hurley, L. Zhang, J. E. Mittler, M. Markowitz, J. P. Moore, A. S. Perelson, and D. D. Ho, Lancet **354**, 1782 (1999).

[82] H. Miao, J. A. Hollenbaugh, M. S. Zand, J. Holden-Wiltse, T. R. Mosmann, A. S. Perelson, H. Wu, and D. J. Topham, J. Virol. **84**, 6687 (2010).

[83] A. S. Perelson, A. U. Neumann, M. Markowitz, J. M. Leonard, and D. D. Ho, Science **271**, 1582 (1996).

[84] S. Bonhoeffer, G. A. Funk, H. F. Gunthard, M. Fischer, and V. Muller, Trends Microbiol. **11**, 499 (2003).

[85] R. R. Regoes, D. L. Barber, R. Ahmed, and R. Antia, Proc. Natl. Acad. Sci. USA **104**, 1599 (2007).

[86] V. V. Ganusov and R. J. De Boer, J. Virol. **82**, 11749 (2008).

[87] V. V. Ganusov, A. E. Lukacher, and A. M. Byers, Virology **405**, 193 (2010).

[88] S. Budhu, J. D. Loike, A. Pandolfi, S. Han, G. Catalano, A. Constantinescu, R. Clynes, and S. C. Silverstein, J. Exp. Med. **207**, 223 (2010).

[89] C. L. Althaus, V. V. Ganusov, and R. J. De Boer, J. Immunol. **179**, 2944 (2007).

[90] R. J. De Boer, M. Oprea, R. Antia, K. Murali-Krishna, R. Ahmed, and A. S. Perelson, J. Virol. **75**, 10663 (2001).

[91] R. J. De Boer, D. Homann, and A. S. Perelson, J. Immunol. **171**, 3928 (2003).

[92] M. P. Davenport, R. M. Ribeiro, and A. S. Perelson, J. Virol. **78**, 10096 (2004).

[93] V. V. Ganusov, J. Immunol. **179**, 5006 (2007).

[94] J. Benichou, R. Ben-Hamo, Y. Louzoun, and S. Efroni, Immunology **135**, 183 (2012).

[95] R. M. Ribeiro, L. Qin, L. L. Chavez, D. Li, S. G. Self, and A. S. Perelson, J. Virol. **84**, 6096 (2010).

[96] P. Baccam, C. Beauchemin, C. A. Macken, F. G. Hayden, and A. S. Perelson, J. Virol. **80**, 7590 (2006).